# Mechanistic Modeling of Vorticity-Facilitated Platelet Aggregation in Stenotic Expansions

Niksa Mohammadi Bagheri[1][0000−0002−6530−7551] and Gabor Závodszky[1,2][0000−0003−0150−0229]

[1] Computational Science Lab, Informatics Institute, University of Amsterdam, Amsterdam, The Netherlands
[2] Department of Hydrodynamic Systems, Faculty of Mechanical Engineering, Budapest University of Technology and Economics, Műegyetem rkp 1–3, 1111 Budapest, Hungary
n.mohammadibagheri@uva.nl

**Abstract.** Vortical flow is common in severe arterial stenoses and blood-contacting medical devices, yet its independent contribution to platelet aggregation remains difficult to quantify amid coexisting shear gradients and recirculation. Here we present a three-dimensional continuum-scale computational framework linking local fluid mechanics to early platelet aggregation in a high expansion-ratio double-stenosis microfluidic geometry at arterial wall shear rates of 1,000–5,000 $s^{-1}$. Platelet transport is coupled to mechanosensitive adhesion kinetics representing VWF–GPIb$\alpha$ capture with rolling/translocation followed by $\alpha$IIb$\beta$3 stabilization. Simulations reproduce vorticity-mediated platelet redistribution from the stenosis apex into the post-stenotic expansion, governing aggregate nucleation and spread. High shear recirculation skews patterns downstream, consistent with experiments. Elevating shear to 5,000 $s^{-1}$ amplifies vortex-driven platelet influx, enhancing rolling-platelet supply and yielding faster growth with greater longitudinal expansion than at 1,000 $s^{-1}$. Vorticity thus modulates early aggregate morphology primarily by shaping shear exposure and rolling-platelet transport. This framework establishes a mechanistic basis for predicting vorticity-facilitated arterial thrombosis in complex flows relevant to advanced stenosis and device thrombogenicity.

**Keywords:** Vorticity · Platelet aggregation · Microfluidics · Mechanobiology · Computational modeling · CFD

## 1 Introduction

Arterial thrombosis remains a leading cause of myocardial infarction and ischemic stroke and continues to complicate blood-contacting cardiovascular technologies, including vascular implants and mechanical circulatory support (MCS) systems [1]. Despite advances in antithrombotic therapy and device design, prevention is limited by a narrow therapeutic window between thrombosis suppression and bleeding risk [2] and by the strong dependence of thrombus initiation on the local hemodynamic environment. In arterial flow, platelet-rich thrombi can form through

ICCS Camera Ready Version 2026
To cite this paper please use the final published version:
DOI: 10.1007/978-3-032-29918-5_12

shear-dependent pathways that become dominant at elevated wall shear rates (often $> 1{,}000\ \mathrm{s}^{-1}$) [3]. Early recruitment is frequently activation-independent and proceeds via von Willebrand factor (VWF) binding to platelet glycoprotein Ib$\alpha$ (GPIb$\alpha$), enabling rapid tethering and rolling/translocation under high shear [4]. Subsequent stabilization and consolidation depend on $\alpha$IIb$\beta$3-mediated anchoring through VWF and/or fibrinogen, producing irreversible platelet–platelet cohesion and volumetric growth [5]. This staged sequence—capture, rolling/translocation, and stabilization—implies that distinct flow features can act on different kinetic bottlenecks and thereby shape thrombus growth rate and morphology [6]. However, many shear-based platelet aggregation models implicitly assume that arterial thrombogenicity is governed primarily by shear-derived metrics alone [7, 8].

Physiologic and device-relevant flows rarely exhibit uniform shear. Acceleration and deceleration generate strong shear-rate gradients [9] and extensional components that reorganize near-wall transport, yielding heterogeneous populations of translocating platelets with geometry-dependent lag times [10]. Downstream, flow separation and recirculation [11] produce vortical (rotational) motion that redistributes platelets, modulates replenishment near thrombogenic surfaces, and alters the spatiotemporal supply of platelets to nascent aggregates. Collectively, these features reshape platelet margination, tethering probability, and rolling/translocation trajectories, and can produce nonlinear (often biphasic) growth kinetics even when nominal wall shear rates are similar. Vortical structures are therefore not exceptional; they are expected in advanced stenoses and at blood-contacting device interfaces, including valves, connectors, cannula junctions, and mechanical circulatory support/extracorporeal membrane oxygenation (MCS/ECMO) components [12].

Microfluidic stenosis platforms [13, 14] provide a controlled setting to disentangle these hemodynamic drivers under arterial shear regimes. High expansion-ratio stenotic designs are especially useful because post-stenotic vortex strength and topology can be tuned systematically through the expansion geometry while maintaining experimental tractability. Ren et al. [14] reported pronounced geometry-dependent aggregation, enhanced VWF incorporation, and vorticity-associated differences in growth; importantly, blocking the VWF–GPIb$\alpha$ pathway suppressed aggregation in vortical regions, supporting a mechanosensitive basis for early recruitment under disturbed flow. However, these observations do not yield a quantitative, mechanistic link between local flow topology—including vorticity distribution and the accompanying shear field—and the staged processes of capture, rolling/translocation, stabilization, and three-dimensional aggregate growth.

From a modeling perspective, most computational thrombosis frameworks were developed for low- to moderate-shear regimes dominated by stasis and coagulation and therefore do not explicitly interrogate vorticity under arterial conditions where shear rates exceed $\sim 1{,}000\ \mathrm{s}^{-1}$ [15–23]. Here, we develop a three-dimensional, continuum-scale computational framework for platelet aggregation in a high expansion-ratio, double-stenosis microfluidic configuration designed to

ICCS Camera Ready Version 2026
To cite this paper please use the final published version:
DOI: 10.1007/978-3-032-29918-5_12

generate controlled vortical flow. The model couples platelet advection–diffusion transport to shear-regulated, mechanosensitive adhesion kinetics, representing rapid VWF–GPIb$\alpha$-mediated capture with rolling/translocation followed by $\alpha$IIb$\beta$3-dependent stabilization, and is evaluated over wall shear rates of 1,000–5,000 $s^{-1}$. By combining device-scale flow resolution with mechanistic adhesion kinetics, we establish a quantitative link between vortex topology, platelet supply, spatial deposition patterns, and emergent clot morphology.

## 2 Methodology

We solve a coupled flow–platelet transport–growth problem to predict early platelet aggregation in a stenotic microfluidic geometry with controlled vortex formation (Fig. 1). The simulation is advanced in time with a repeating sequence: (1) compute the device-scale hemodynamics, (2) update platelet transport and shear-regulated adhesion kinetics, and (3) advance the aggregate interface. The updated aggregate geometry modifies the flow through a porous-resistance term, closing the feedback loop between evolving hemodynamics and growth.

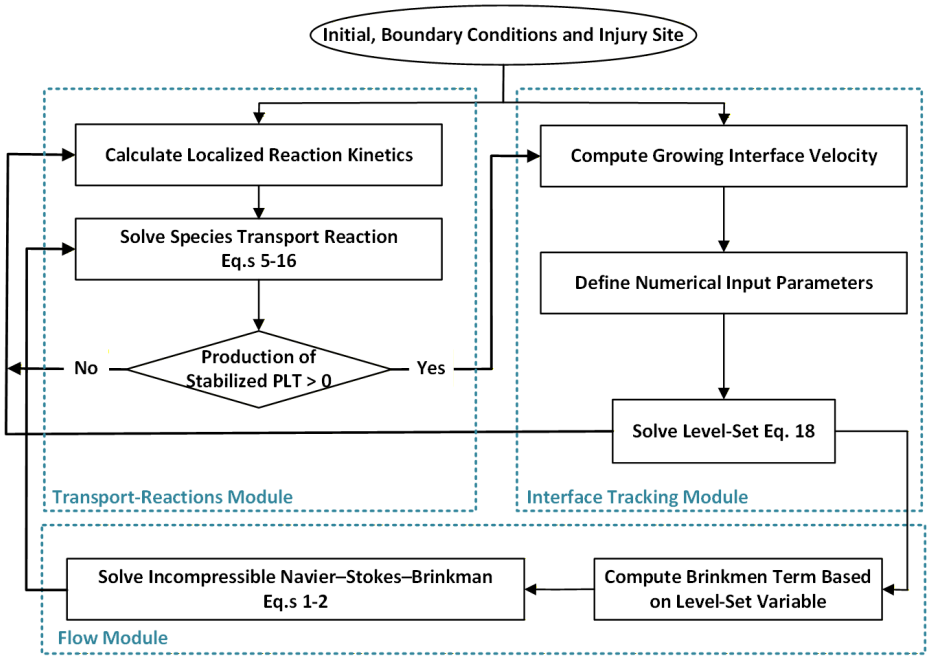


**Fig. 1.** Flowchart of the major steps of the simulation.

ICCS Camera Ready Version 2026
To cite this paper please use the final published version:
DOI: 10.1007/978-3-032-29918-5_12

### 2.1 Hemodynamics

Blood is treated as a single-phase incompressible Newtonian fluid. Flow through the porous aggregate is represented by a Brinkman resistance term that is activated inside the aggregate:

$$\rho\left(\frac{\partial \mathbf{u}}{\partial t} + \mathbf{u}\cdot\nabla\mathbf{u}\right) = -\nabla p + \mu\nabla^2\mathbf{u} - \mu K^{-1}(\phi)\,\mathbf{u}, \tag{1}$$

$$\nabla\cdot\mathbf{u} = 0. \tag{2}$$

Here $\mathbf{u}(\mathbf{x},t)$ is the velocity, $p(\mathbf{x},t)$ is the pressure, $\rho$ is the density, $\mu$ is the dynamic viscosity, and $K(\phi)$ is the permeability. We switch permeability via a smoothed Heaviside function $H_\varepsilon(\phi)$:

$$K^{-1}(\phi) = \frac{1 - H_\varepsilon(\phi)}{K_{\text{clot}}}, \tag{3}$$

so that the Brinkman term is negligible in the lumen ($H_\varepsilon \approx 1$) and active in the aggregate ($H_\varepsilon \approx 0$), with $K_{\text{clot}}$ the aggregate permeability. The regularized Heaviside $H_\varepsilon(\phi)$ is

$$H_\varepsilon(\phi) = \begin{cases} 0, & \phi \le \frac{1}{2} - \varepsilon, \\ \frac{1}{2}\left[1 + \frac{\phi - \frac{1}{2}}{\varepsilon} + \frac{1}{\pi}\sin\left(\pi\frac{\phi - \frac{1}{2}}{\varepsilon}\right)\right], & \left|\phi - \frac{1}{2}\right| < \varepsilon, \\ 1, & \phi \ge \frac{1}{2} + \varepsilon. \end{cases} \tag{4}$$

where $\varepsilon$ sets the half-thickness of the transition band.

### 2.2 Platelet populations and transport

We evolve three platelet populations: (i) free-flowing platelets $c_f(\mathbf{x},t)$ in the lumen; (ii) rolling/translocating platelets $c_r(\mathbf{x},t)$ confined to a near-thrombogenic wall tether layer and to the clot–fluid interfacial band; and (iii) stabilized platelets $c_s(\mathbf{x},t)$ that drive growth. Free platelets undergo advection–diffusion in the lumen, while rolling platelets are transported tangentially along aggregate surface and near-thrombogenic walls and can irreversibly stabilize with a shear-dependent rate:

$$\frac{\partial c_f}{\partial t} + H_\varepsilon(\phi)\,\mathbf{u}\cdot\nabla c_f = H_\varepsilon(\phi)\,\nabla\cdot(D\nabla c_f) - R_b, \tag{5}$$

where $D$ is a platelet diffusivity. The only volumetric sink is $R_b$, which represents capture from the lumen into the rolling pool at the aggregate surface. Conversion at the thrombogenic wall is imposed as a boundary flux (Eq. (8)); for the impact of boundary fluxes in deriving accumulation of platelets see [24].

Interfacial capture is localized to the band around $\phi = \frac{1}{2}$ using a band-limited interface indicator $\delta_\varepsilon(\phi)$:

$$R_b = \beta\,\delta_\varepsilon(\phi)\,c_f\left(1 - \frac{c_r}{c_{\max}}\right), \tag{6}$$

ICCS Camera Ready Version 2026
To cite this paper please use the final published version:
DOI: 10.1007/978-3-032-29918-5_12

where $\beta$ is a capture rate, $c_{\max}$ is an effective saturation level for rolling sites, and

$$\delta_\varepsilon(\phi) = 6\,|\nabla\phi|\,\phi(1-\phi), \tag{7}$$

which is nonzero only within the diffuse interfacial band.

On the thrombogenic wall $\Gamma_w$, free-flowing platelets are converted to rolling platelets via a first-order flux that activates only above a wall-shear threshold $\dot{\gamma}_{\text{th}} = 1000\ \text{s}^{-1}$, see [3]:

$$-\mathbf{n}\cdot D\nabla c_f\big|_{\Gamma_w} = J_w = k_w\,H(\dot{\gamma}_w - \dot{\gamma}_{\text{th}})\,c_f\left(1-\frac{c_r}{c_{\max}}\right)\Big|_{\Gamma_w}, \tag{8}$$

where $\mathbf{n}$ is the outward unit normal, $k_w$ is a thrombogenic wall binding rate [19, 22], $\dot{\gamma}_w$ is the local wall shear rate, and $H(\cdot)$ is the Heaviside step function.

Rolling/translocating platelets are restricted to a VWF-mediated near-wall tether layer of thickness $l_t = 15\ \mu$m [4, 6]. Using a Heaviside switch based on the wall-normal distance $d_w(\mathbf{x})$ to the thrombogenic wall $\Gamma_w$, we define

$$H_t(\mathbf{x}) \equiv H(l_t - d_w(\mathbf{x}))\,, \tag{9}$$

so that $H_t = 1$ inside the tether layer and $H_t = 0$ outside. The rolling (translocation) velocity is prescribed as

$$\mathbf{u}_r(\mathbf{x}) = 0.02\,H_t(\mathbf{x})\,\mathbf{u}_\tau(\mathbf{x}), \qquad \mathbf{u}_\tau = \mathbf{u} - (\mathbf{u}\cdot\mathbf{n})\mathbf{n}, \tag{10}$$

where platelets translocate at 2% of the local tangential flow speed within $l_t$ of $\Gamma_w$, and $\mathbf{u}_r = 0$ otherwise.

We define a smooth interfacial band indicator

$$H_r(\phi) = \begin{cases} 0, & \phi < 0.1, \\ \frac{1}{2}\left[1+\sin\left(\pi\dfrac{\phi-0.5}{0.4}\right)\right], & 0.1 \le \phi \le 0.9, \\ 0, & \phi > 0.9, \end{cases} \tag{11}$$

and evolve $c_r$ as

$$\frac{\partial c_r}{\partial t} + H_r(\phi)\,\mathbf{u}_r\cdot\nabla c_r = H_r(\phi)\,\nabla\cdot(D\nabla c_r) + R_b - k_{\text{adh}}(\dot{\gamma})\,c_r. \tag{12}$$

Here $k_{\text{adh}}(\dot{\gamma})$ is the shear-regulated stabilization rate. Free-flowing platelets are converting into the rolling pool through the boundary flux condition of

$$-\mathbf{n}\cdot D_r\nabla c_r\big|_{\Gamma_w} = -J_w. \tag{13}$$

The local shear rate used in mechanosensitive kinetics is defined as

$$\dot{\gamma} = \sqrt{2\,\mathbf{D}:\mathbf{D}}, \qquad \mathbf{D} = \tfrac{1}{2}\left(\nabla\mathbf{u} + (\nabla\mathbf{u})^T\right). \tag{14}$$

Rolling platelets stabilize with a Hill-type shear switch:

$$k_{\text{adh}}(\dot{\gamma}) = a_{\text{low}}(1-\varphi_s) + a_{\text{high}}\varphi_s, \qquad \varphi_s = \frac{\dot{\gamma}^2}{\dot{\gamma}^2 + \dot{\gamma}_c^2}, \tag{15}$$

ICCS Camera Ready Version 2026
To cite this paper please use the final published version:
DOI: 10.1007/978-3-032-29918-5_12

where $a_{\text{low}}$ and $a_{\text{high}}$ are limiting stabilization rates and $\dot{\gamma}_c$ is a characteristic shear rate for pathway switching. Stabilized platelet production is

$$\frac{\partial c_s}{\partial t} = k_{\text{adh}}(\dot{\gamma})\, c_r. \tag{16}$$

### 2.3 Aggregate growth (conservative level-set method)

The clot–lumen interface is represented by $\phi(\mathbf{x}, t) \in [0, 1]$, with $\phi \approx 0$ in the aggregate and $\phi \approx 1$ in the fluid; the interface is $\phi = \frac{1}{2}$. The outward unit normal is

$$\mathbf{n} = \frac{\nabla\phi}{|\nabla\phi|}. \tag{17}$$

Interface motion is governed by a conservative level-set equation with a prescribed normal growth speed $V_n$:

$$\frac{\partial\phi}{\partial t} + \mathbf{u}_g \cdot \nabla\phi = \gamma_{\text{ls}} \nabla \cdot (\varepsilon_{\text{ls}} \nabla\phi - \phi(1-\phi)\mathbf{n}), \qquad \mathbf{u}_g = H_r(\phi)\, V_n\, \mathbf{n}. \tag{18}$$

Here, $\varepsilon_{\text{ls}}$ sets the interface thickness and $\gamma_{\text{ls}}$ controls regularization/reinitialization; $H_r(\phi)$ restricts advection to the interfacial band. The normal growth speed is obtained from stabilization of rolling platelets:

$$J_s = k_{\text{adh}}(\dot{\gamma})\, c_r\, l_{\text{ptr}}, \qquad V_n^0 = J_s\, v_{\text{plt}}\, (1 + \alpha_s), \tag{19}$$

where $J_s$ is the stabilized platelet flux, $l_{\text{ptr}}$ is an effective interaction-layer thickness, $v_{\text{plt}}$ is platelet volume, and $\alpha_s$ accounts for packing/porosity. We suppress aggregate advancement above an upper shear threshold to reflect mechanically unstable growth in the early-time window [6]. Specifically,

$$V_n = V_n^0\, [1 - H(\dot{\gamma}_w - \dot{\gamma}_{\text{stop}})], \tag{20}$$

where $\dot{\gamma}_{\text{stop}} = 10^4\ \text{s}^{-1}$. For $\dot{\gamma}_w > \dot{\gamma}_{\text{stop}}$, $V_n = 0$ and the interface is not updated.

### 2.4 Initial and boundary conditions

The volumetric flow rate was chosen for each geometry to impose target inlet wall shear rates of $\dot{\gamma}_0 = 1{,}000$ and $5{,}000\ \text{s}^{-1}$. To reduce computational cost, only half of the channel was simulated, justified by geometric and flow symmetry in the CFD solutions. On the symmetry plane $\Gamma_{\text{sym}}$ we impose:

$$\mathbf{u} \cdot \mathbf{n} = 0, \quad \mathbf{n} \cdot \boldsymbol{\sigma} \cdot \mathbf{t} = 0, \quad \nabla c_f \cdot \mathbf{n} = 0, \qquad \text{on } \Gamma_{\text{sym}}, \tag{21}$$

where $\boldsymbol{\sigma}$ is the Cauchy stress tensor and $\mathbf{t}$ denotes any tangential direction. At the inlet $\Gamma_{\text{in}}$, we prescribe

$$\mathbf{u} = \mathbf{u}_{\text{in}}, \qquad c_f = c_{f,\text{in}}, \qquad \text{on } \Gamma_{\text{in}}. \tag{22}$$

ICCS Camera Ready Version 2026
To cite this paper please use the final published version:
DOI: 10.1007/978-3-032-29918-5_12

**Table 1.** Parameters used in simulations.

| Symbol | Description | Value | Unit | Ref. |
|---|---|---|---|---|
| $\rho$ | Density of fluid | $1.025 \times 10^3$ | $\mathrm{kg\,m^{-3}}$ | [13] |
| $\mu$ | Fluid viscosity | $3 \times 10^{-3}$ | $\mathrm{Pa\,s}$ | [13] |
| $K_{\mathrm{clot}}$ | Aggregate permeability | $3.5 \times 10^{-14}$ | $\mathrm{m^2}$ | [25] |
| $D$ | Platelet diffusivity | $2 \times 10^{-11}$ | $\mathrm{m^2\,s^{-1}}$ | [20] |
| $c_{\max}$ | Maximum PLT concentration in space | $2.5 \times 10^{16}$ | $\mathrm{Plt\,m^{-3}}$ | [26] |
| $\beta$ | Free-flowing PLT capture rate | 0.02 | $\mathrm{s^{-1}}$ | [27, 28] |
| $k_w$ | Thrombogenic wall binding rate | 0.001 | $\mathrm{m\,s^{-1}}$ | [22] |
| $a_{\mathrm{low}}$ | Low-shear stabilization rate | 2 | $\mathrm{s^{-1}}$ | [29] |
| $a_{\mathrm{high}}$ | High-shear stabilization rate | 4 | $\mathrm{s^{-1}}$ | [29] |
| $\dot{\gamma}_c$ | Critical shear rate (switch) | 3000 | $\mathrm{s^{-1}}$ | [4, 30] |

Because platelet margination is not modeled explicitly, an effective inlet platelet concentration is used [14]:

$$c_{f,\mathrm{in}} = \begin{cases} 1.0 \times 10^{14}\ \mathrm{m^{-3}}, & \dot{\gamma}_0 = 1{,}000\ \mathrm{s^{-1}}, \\ 3.0 \times 10^{14}\ \mathrm{m^{-3}}, & \dot{\gamma}_0 = 5{,}000\ \mathrm{s^{-1}}. \end{cases} \tag{23}$$

At the outlet $\Gamma_{\mathrm{out}}$, a reference pressure is set and a zero diffusive-flux condition is applied for platelet transport:

$$p = 0, \qquad -D\nabla c_f \cdot \mathbf{n} = 0, \qquad \text{on } \Gamma_{\mathrm{out}}. \tag{24}$$

On non-thrombogenic walls, we enforce no-flux for $c_f$:

$$-D\nabla c_f \cdot \mathbf{n} = 0. \tag{25}$$

On the thrombogenic wall $\Gamma_w$, platelet capture is imposed through the shear-thresholded flux in Eq. (8). Figure 2 demonstrates the simulation setup (right), the corresponding microfluidic channel (middle), and the *in vivo* condition (left).

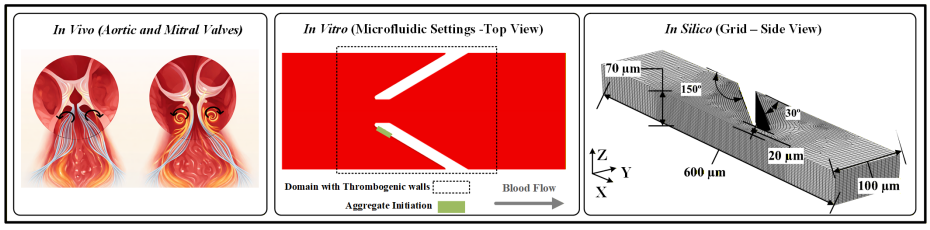


**Fig. 2.** Experimental (*in vitro* measurements taken from [14]) and computational setups mimicking pathologic arterial flow configurations.

The clot–lumen interface is represented by $\phi(\mathbf{x}, t)$, with the interface at $\phi = 0.5$. Here, a conservative level-set formulation was adopted over phase-field because the explicit $\phi = 0.5$ isosurface enables direct aggregate geometry

ICCS Camera Ready Version 2026
To cite this paper please use the final published version:
DOI: 10.1007/978-3-032-29918-5_12

extraction and validation against *in vitro* measurements, with inherent volume conservation and no additional Cahn–Hilliard parameter calibration required. All simulations were performed in COMSOL Multiphysics (v6.2) using the finite-element method on an Intel Core i9-10980XE workstation (18 cores, 3.0 GHz, 128 GB RAM). The computational domain was discretized with approximately $6.4 \times 10^4$ hexahedral elements, refined in the stenosis/expansion region and across the diffuse level-set band to ensure at least three elements spanned the interface thickness. Mesh convergence was verified by refinement until peak wall shear rate and wall platelet flux changed by $< 5\%$. The segregated solver combined GMRES with AMG preconditioning for the coupled flow and transport equations, and PARDISO for the level-set update. Time integration employed an implicit BDF scheme with adaptive stepping. Each 4-minute physical-time simulation completed in approximately 22 minutes, with peak memory usage of 7.8 GB. The principal numerical sensitivity of the coupled formulation was associated with the conservative level-set regularization, for which the interface thickness $\varepsilon$ was selected proportional to the local element size to ensure resolution by at least three elements, and the reinitialization parameter $\gamma$ was scaled to the maximum platelet-flux-driven interface velocity. This approach maintained interface sharpness and numerical stability during aggregate growth without requiring adaptive remeshing. Under these settings, the coupled solver converged robustly within the segregated implicit BDF framework.

## 3 Results and Discussion

To examine how arterial shear rate modulates vorticity-driven platelet aggregation under complex flow conditions relevant to the aorta and valve outflow (Fig. 2), we performed three-dimensional CFD simulations in a high expansion-ratio, double-stenosis microfluidic channel with a fixed post-stenotic expansion angle of 150° (Fig. 2). The inlet flow rate was adjusted to impose two wall shear-rate conditions (WSR = 1,000 and 5,000 $s^{-1}$). For each shear condition, the predicted flow field, translocating platelet distribution, and aggregate formation were evaluated over 4 min, and the resulting three-dimensional aggregate growth and morphology were compared with corresponding *in vitro* microfluidic measurements [14].

In evaluating aggregate growth dynamics under distinct shear conditions, Fig. 3 illustrates the time evolution at WSR = 1,000 $s^{-1}$. At the initial time and at $t = 240$ s, top and side views show steady aggregate formation with limited downstream extension. The post-stenotic expansion generates a stable separation bubble and recirculation layer behind the constriction, which increases near-wall residence and platelet–wall re-encounter frequency, but does not strongly focus transport to a distal attachment front. Accordingly, translocating platelets accumulate gradually and remain comparatively diffuse, producing a less sharply defined platelet "envelope" around the growing clot. Streamline penetration into the developing porous aggregate is minimal (red arrows in Fig. 3), indicating that early growth is dominated by near-surface rolling/capture rather than by appreciable intra-aggregate advection. By contrast, Fig. 4 (WSR = 5,000 $s^{-1}$)

ICCS Camera Ready Version 2026
To cite this paper please use the final published version:
DOI: 10.1007/978-3-032-29918-5_12

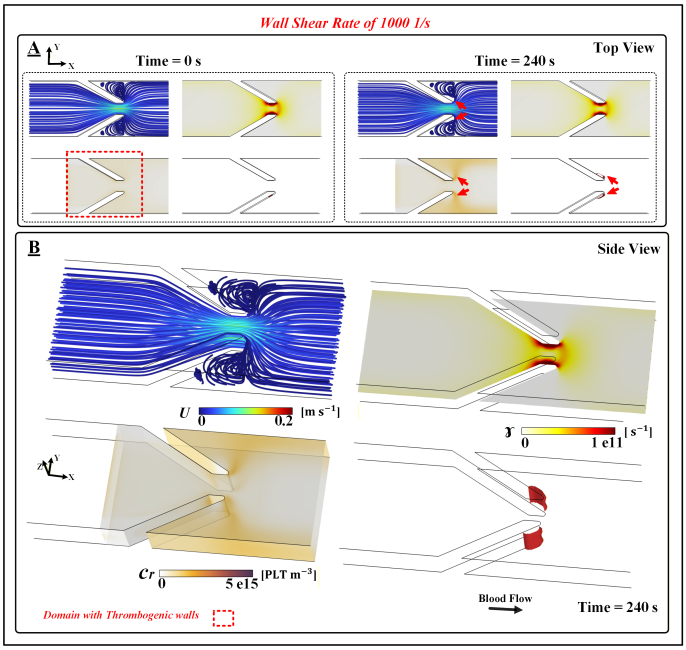


**Fig. 3.** Hemodynamic features and aggregate evolution at WSR = 1,000 $s^{-1}$.

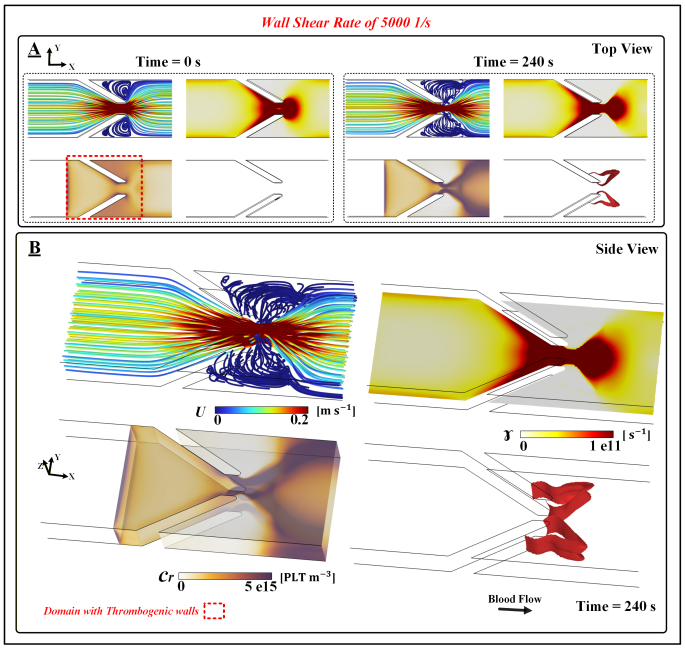


**Fig. 4.** Hemodynamic features and aggregate evolution at WSR = 5,000 $s^{-1}$.

ICCS Camera Ready Version 2026
To cite this paper please use the final published version:
DOI: 10.1007/978-3-032-29918-5_12

demonstrates faster aggregate progression and a clear downstream bias in morphology. With higher inflow, the adverse pressure gradient across the expansion intensifies and the post-stenotic shear layers strengthen, expanding the recirculation footprint and increasing streamline deflection. At $t = 240$ s, translocating platelets are highly concentrated near the stenosis and form a dense layer that closely follows the aggregate surface, consistent with enhanced near-wall delivery and retention along the recirculation boundary. Notably, at high shear the porous nature of the developing aggregate permits minor streamline penetration into the clot region (Fig. 4). This is consistent with weak perfusion through a permeable porous structure: the larger imposed flow rate increases the pressure drop across the clot-facing region and drives nonzero seepage through the porous-resistance formulation, whereas at 1,000 $s^{-1}$ the same permeability yields negligible penetration.

Initially, in both low and high shear conditions, vortices formed behind the constriction, with local stenosis shear rates exceeding 10,000 $s^{-1}$. At 1,000 $s^{-1}$, this peak-shear zone remains confined near the stenosis, whereas at 5,000 $s^{-1}$ it expands both downstream and upstream and reorganizes the near-wall transport pathway. At 5,000 $s^{-1}$ the post-stenotic high-shear footprint (local WSR >10,000 $s^{-1}$) reshapes translocating platelet accumulation and, in turn, the trajectory of aggregate growth. Aggregate formation was not observed within the >10,000 $s^{-1}$ band itself, consistent with the stopping shear threshold used in the growth model. Instead, growth localized to the second half of the post-stenotic region where shear remained elevated (WSR >1,000 $s^{-1}$; Fig. 4), sufficient to promote VWF-mediated platelet tethering and capture, yet below peak stenotic shear. As a result, the aggregate tracked the outer edge of the peak-shear zone and propagated along the upper boundary of the recirculation layer, producing a downstream-skewed morphology rather than expanding into the vortex core. In parallel, translocating platelets formed a dense, surface-aligned layer and—under the higher inflow at 5,000 $s^{-1}$—were preferentially delivered to and retained near the wall. Together, these mechanisms promote thrombogenic, wall-directed downstream propagation while maintaining a preference for growth within elevated shear regions below 10,000 $s^{-1}$. Within this shear window, the combination of sustained rolling-platelet availability and repeated platelet–surface encounters supports stable accumulation in the absence of fibrin formation, whereas the peak-shear band is not permissive for growth in the present formulation.

Quantitatively, the higher shear condition exhibited an approximately fivefold increase in translocating platelet concentration compared with the lower shear condition. In this study, that amplification reflects both flow-driven changes in near-wall delivery/retention associated with the stronger post-stenotic recirculation topology and the higher prescribed inlet platelet concentration used for the 5,000 $s^{-1}$ case to represent increased near-wall platelet availability not explicitly captured (e.g., RBC-mediated margination). Additionally, the vortical region at 5,000 $s^{-1}$ expands downstream over time, whereas at 1,000 $s^{-1}$ it remains largely unchanged, correlating with enhanced aggregate longitudinal expansion and downstream inclination.

ICCS Camera Ready Version 2026
To cite this paper please use the final published version:
DOI: 10.1007/978-3-032-29918-5_12

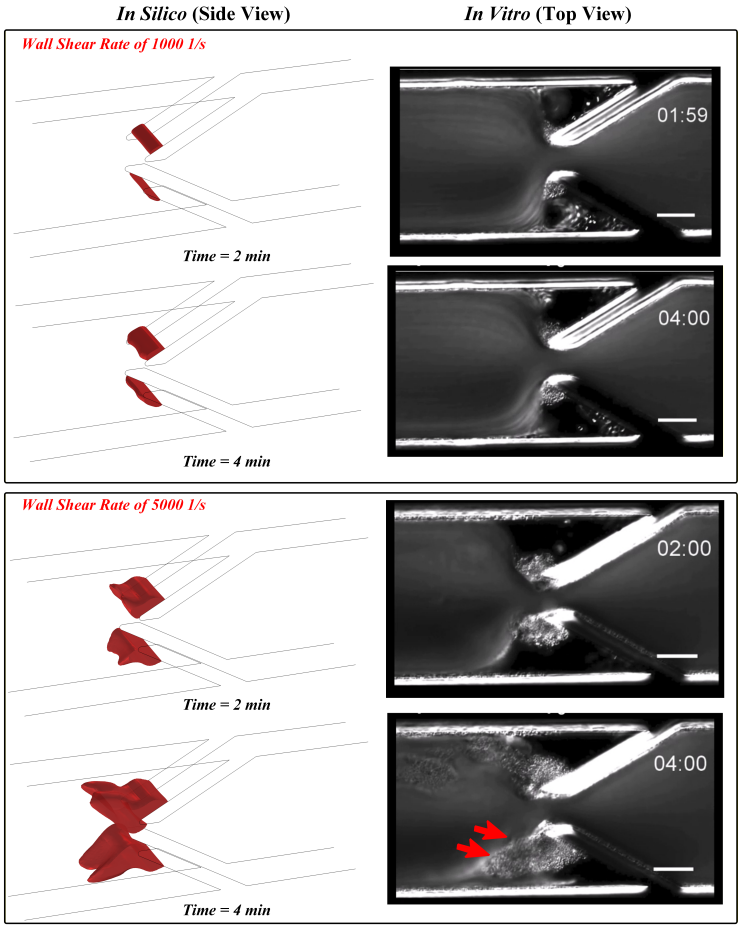


**Fig. 5.** Comparison of aggregate growth dynamics and morphology over 4 min at WSR = 1,000 and 5,000 $s^{-1}$ with *in vitro* measurements [14].

ICCS Camera Ready Version 2026
To cite this paper please use the final published version:
DOI: 10.1007/978-3-032-29918-5_12

In arterial thrombosis, VWF–GPIb$\alpha$-mediated platelet rolling constitutes the rate-limiting step preceding $\alpha$IIb$\beta$3-dependent firm adhesion [4]. We therefore emphasize the rolling/translocating concentration $c_r$ as the central diagnostic variable: unlike bulk free-flowing platelets ($c_f$, relatively uniform in the lumen) or stabilized platelets ($c_s$, confined to the aggregate interior), $c_r$ localizes precisely to the shear-regulated growth interface (Eq. 11) where near-wall transport directly feeds mechanosensitive adhesion kinetics. Quantitatively, peak $c_r$ increased 5-fold from $1 \times 10^{15}$ m$^{-3}$ at WSR = 1,000 s$^{-1}$ to $5 \times 10^{15}$ m$^{-3}$ at WSR = 5,000 s$^{-1}$ (Figs. 3–4), demonstrating that post-stenotic recirculation reorganizes near-wall platelet supply and governs the downstream-skewed aggregate morphology observed experimentally [14].

In the final comparison (Fig. 5), aggregate volume and surface coverage were assessed against *in vitro* measurements over 4 min. At WSR = 1,000 s$^{-1}$, aggregate volume increased modestly between 2 and 4 min and remained near the wall behind the stenosis. In contrast, at WSR = 5,000 s$^{-1}$, aggregate volume increased substantially over the same interval and closely followed *in vitro* trends. As indicated by the red arrow in Fig. 5, the 5,000 s$^{-1}$ aggregate inclined downstream toward the wall rather than spreading upstream, consistent with experimental observations. Simulations also revealed wall-biased growth, with more pronounced accumulation near the top and bottom walls and reduced growth at the center—especially at 5,000 s$^{-1}$.

The current framework deliberately isolates early shear-mediated platelet adhesion and transport, consistent with the SIPA conditions of the *in vitro* validation experiments [14] where fibrin formation is negligible over the 4-min observation window. Explicit shear-induced detachment kinetics at extreme shear (>10,000 s$^{-1}$) and RBC-mediated margination are not incorporated. Blood is treated as Newtonian ($\mu = 3 \times 10^{-3}$ Pa·s); since wall shear rates exceed 1,000 s$^{-1}$ throughout the thrombogenic region, shear-thinning effects introduce <10% error in shear magnitude [31, 32]. Aggregate permeability is held constant, representative of loosely packed early aggregates [25]; platelet contraction and fibrin crosslinking would reduce permeability during later consolidation phases [33], altering intra-aggregate perfusion and surface shear. At longer time scales (>5–10 min) or under coagulation-promoting conditions, fibrin polymerization and progressive lumen narrowing would modify the vorticity-driven transport mechanisms identified here. The observed wall-biased growth is interpreted as a near-wall transport effect; cell-scale margination in whole blood would likely reinforce this peripheral asymmetry.

## 4 Conclusion

This study establishes a validated three-dimensional CFD–thrombosis framework that mechanistically links post-stenotic vortical flow to early platelet aggregation. Across arterial shear conditions (WSR = 1,000–5,000 s$^{-1}$), the recirculation boundary organizes a wall-directed transport corridor that concentrates rolling platelets along the distal growth front, producing the downstream-skewed aggre-

ICCS Camera Ready Version 2026
To cite this paper please use the final published version:
DOI: 10.1007/978-3-032-29918-5_12

gate morphology observed experimentally. A 5-fold enhancement in rolling-platelet delivery at elevated shear drives accelerated longitudinal expansion in quantitative agreement with microfluidic measurements. These findings demonstrate that disturbed-flow topology—not shear magnitude alone—is a primary determinant of early thrombus architecture. The framework provides a predictive platform for evaluating thrombogenic risk in stenotic arteries and optimizing blood-contacting medical device geometries.

**Disclosure of Interests.** The authors have no competing interests to declare that are relevant to the content of this article.

## References


1. Jackson, S.P.: Arterial thrombosis—insidious, unpredictable and deadly. *Nature Medicine* **17**(11), 1423–1436 (2011). https://doi.org/10.1038/nm.2515
2. Anjum, M., et al.: Stroke and bleeding risk in atrial fibrillation with $CHA_2DS_2$-VASC risk score of one: the Norwegian AFNOR study. *European Heart Journal* **45**(1), 57–66 (2024). https://doi.org/10.1093/eurheartj/ehad659
3. Ruggeri, Z.M.: Platelet adhesion under flow. *Microcirculation* **16**(1), 58–83 (2009). https://doi.org/10.1080/10739680802651477
4. Dopheide, S.M., Maxwell, M.J., Jackson, S.P.: Shear-dependent tether formation during platelet translocation on von Willebrand factor. *Blood* **99**(1), 159–167 (2002). https://doi.org/10.1182/blood.v99.1.159
5. Maxwell, M.J., Westein, E., Nesbitt, W.S., Giuliano, S., Dopheide, S.M., Jackson, S.P.: Identification of a 2-stage platelet aggregation process mediating shear-dependent thrombus formation. *Blood* **109**(2), 566–576 (2007). https://doi.org/10.1182/blood-2006-07-028282
6. Receveur, N., Nechipurenko, D., Knapp, Y., Panteleev, M., Gachet, C., Mangin, P.H.: Shear rate gradients promote a bi-phasic thrombus formation on weak adhesive proteins, such as fibrinogen in a von Willebrand factor-dependent manner. *Haematologica* **105**(10), 2471–2483 (2020). https://doi.org/10.3324/haematol.2019.235754
7. Rana, A., Westein, E., Niego, B., Hagemeyer, C.E.: Shear-dependent platelet aggregation: Mechanisms and therapeutic opportunities. *Frontiers in Cardiovascular Medicine* **6**, 141 (2019). https://doi.org/10.3389/fcvm.2019.00141
8. Tuna, R., Yi, W., Crespo Cruz, E., et al.: Platelet biorheology and mechanobiology in thrombosis and hemostasis: Perspectives from multiscale computation. *International Journal of Molecular Sciences* **25**(9), 4800 (2024). https://doi.org/10.3390/ijms25094800
9. Nesbitt, W.S., Westein, E., Tovar-Lopez, F.J., et al.: A shear gradient–dependent platelet aggregation mechanism drives thrombus formation. *Nature Medicine* **15**(6), 665–673 (2009). https://doi.org/10.1038/nm.1955
10. Liu, Z.L., Bresette, C., Aidun, C.K., Ku, D.N.: SIPA in 10 milliseconds: VWF tentacles agglomerate and capture platelets under high shear. *Blood Advances* **6**(8), 2453–2465 (2022). https://doi.org/10.1182/bloodadvances.2021005692
11. Ciuti, M., Zampogna, G.A., Gallaire, F., Camarri, S., Ledda, P.G.: On the effect of a penetrating recirculation region on the bifurcations of the flow past a permeable sphere. *Physics of Fluids* **33**(12), 124103 (2021). https://doi.org/10.1063/5.0075244


ICCS Camera Ready Version 2026
To cite this paper please use the final published version:
DOI: 10.1007/978-3-032-29918-5_12

12. Sun, A., Nasser, A., Yap, N.A., Gao, R., Ju, L.A.: 3M engineering approaches to combat high-shear thrombosis: Integrating modeling, microfluidics, and mechanobiology. *Current Opinion in Biomedical Engineering* **33**, 100576 (2025). https://doi.org/10.1016/j.cobme.2025.100576
13. van Rooij, B.J.M., Závodszky, G., Hoekstra, A.G., Ku, D.N.: Biorheology of occlusive thrombi formation under high shear: *in vitro* growth and shrinkage. *Scientific Reports* **10**(1), 1–11 (2020). https://doi.org/10.1038/s41598-020-74518-7
14. Ren, J., Abidin, N.A.Z., Sun, A., et al.: Vorticity-facilitated platelet aggregation: a high expansion-ratio stenotic microfluidic platform unravels the role of complex flow dynamics in arterial thrombosis. *Advanced Healthcare Materials* **14**(28), e2500436 (2025). https://doi.org/10.1002/adhm.202500436
15. Menichini, C., Cheng, Z., Gibbs, R.G.J.J., Xu, X.Y.: Predicting false lumen thrombosis in patient-specific models of aortic dissection. *Journal of the Royal Society Interface* **13**(124) (2016). https://doi.org/10.1098/rsif.2016.0759
16. Leiderman, K., Fogelson, A.L.: Grow with the flow: A spatial-temporal model of platelet deposition and blood coagulation under flow. *Mathematical Medicine and Biology* **28**(1), 47–84 (2011). https://doi.org/10.1093/imammb/dqq005
17. Govindarajan, V., Zhu, S., Li, R., et al.: Impact of tissue factor localization on blood clot structure and resistance under venous shear. *Biophysical Journal* **114**(4), 978–991 (2018). https://doi.org/10.1016/j.bpj.2017.12.034
18. Bouchnita, A., Galochkina, T., Kurbatova, P., Nony, P., Volpert, V.: Conditions of microvessel occlusion for blood coagulation in flow. *International Journal for Numerical Methods in Biomedical Engineering* **33**(9) (2017). https://doi.org/10.1002/cnm.2850
19. Sorensen, E.N., Burgreen, G.W., Wagner, W.R., et al.: Computational simulation of platelet deposition and activation: I. Model development and properties. *Annals of Biomedical Engineering* **27**(4), 436–448 (1999). https://doi.org/10.1114/1.200
20. Storti, F., van Kempen, T.H.S., van de Vosse, F.N.: A continuum model for platelet plug formation and growth. *International Journal for Numerical Methods in Biomedical Engineering* **30**(6), 634–658 (2014). https://doi.org/10.1002/cnm.2623
21. Armour, C.H., Menichini, C., Hanna, L., Gibbs, R.G.J., Xu, X.Y.: Computational modeling of flow and thrombus formation in type B aortic dissection: The influence of false lumen perfused side branches. *Studies in Mechanobiology, Tissue Engineering and Biomaterials* **24**, 53–72 (2022). https://doi.org/10.1007/978-3-030-92339-6_2
22. Bark, D.L., Ku, D.N.: Platelet transport rates and binding kinetics at high shear over a thrombus. *Biophysical Journal* **105**(2), 502–511 (2013)
23. Sarrami-Foroushani, A., Lassila, T., Hejazi, S.M., Nagaraja, S., Bacon, A., Frangi, A.F.: A computational model for prediction of clot platelet content in flow-diverted intracranial aneurysms. *Journal of Biomechanics* **91**, 7–13 (2019). https://doi.org/10.1016/j.jbiomech.2019.04.045
24. Bagheri, N.M., Závodszky, G., Hoekstra, A.G.: The impact of clot permeability on platelet fluxes toward its surface. *PLOS ONE* **20**(3), e0317828 (2025). https://doi.org/10.1371/journal.pone.0317828
25. Du, J., Kim, D., Alhawael, G., Ku, D.N., Fogelson, A.L.: Clot permeability, agonist transport, and platelet binding kinetics in arterial thrombosis. *Biophysical Journal* **119**(10), 2102–2115 (2020). https://doi.org/10.1016/j.bpj.2020.08.041
26. Wu, W., Jamiolkowski, M.A., Wagner, W.R., Aubry, N., Massoudi, M., Antaki, J.F.: Multi-constituent simulation of thrombus deposition. *Scientific Reports* **7**, 42720 (2017). https://doi.org/10.1038/srep42720
27. Savage, B., Saldivar, E., Ruggeri, Z.M.: Initiation of platelet adhesion by arrest onto fibrinogen or translocation on von Willebrand factor. *Cell* **84**, 289–297 (1996)

ICCS Camera Ready Version 2026
To cite this paper please use the final published version:
DOI: 10.1007/978-3-032-29918-5_12

28. Butakov, I., Terekhov, K., Vassilevski, Y.: A Simple Model of White Clot Formation. *Mathematical Models and Computer Simulations* **46**(1), 177–189 (2025). https://doi.org/10.1134/S199508022460849X
29. Bagheri, N.M., Závodszky, G., Hoekstra, A.G.: Shear-regulated transport–reaction modeling of platelet translocation and aggregation in heterogeneous arterial microflows: a 3D continuum framework. Submitted (2026)
30. Yeo, E.F., Oliver, J.M., Korin, N., Waters, S.L.: A continuum model for the elongation and orientation of von Willebrand factor with applications in arterial flow. *Biomechanics and Modeling in Mechanobiology* **23**(4), 1299–1317 (2024). https://doi.org/10.1007/s10237-024-01840-8
31. Cho, Y.I., Kensey, K.R.: Effects of the non-Newtonian viscosity of blood on flows in a diseased arterial vessel. Part 1: Steady flows. *Biorheology* **28**(3–4), 241–262 (1991)
32. Johnston, B.M., Johnston, P.R., Corney, S., Kilpatrick, D.: Non-Newtonian blood flow in human right coronary arteries: steady state simulations. *Journal of Biomechanics* **37**(5), 709–720 (2004)
33. Wufsus, A.R., Macera, N.E., Neeves, K.B.: The hydraulic permeability of blood clots as a function of fibrin and platelet density. *Biophysical Journal* **108**(7), 1648–1658 (2015)

ICCS Camera Ready Version 2026
To cite this paper please use the final published version:
DOI: 10.1007/978-3-032-29918-5_12